Technology Explanation

Characteristics Prediction of Vane Pump by CFD Analysis

SUZUKI Kazunari, NAKAMURA Yoshinari, YAKABE Sinji,
WATANABE Hirohito, NAKAMURA Kazuhisa

Abstract

Due to the reduction in vehicle fuel consumption in recent years, a need has arisen for high-speed rotation and miniaturization of vane pumps for in-vehicle use. CFD analysis can be utilized as one effective tool for meeting higher performance requirements in pump design and development. In order to improve pump performance, it is important to precisely predict pump characteristics, such as the rotational speed/flow rate characteristic, and the internal pressure in the vane chamber. However, when a pump is driven at high rotational speed, prediction of pump characteristics is often difficult due to behavior of gases contained in the oil. A precise model for CFD analysis must be derived to capture the actual phenomena in the vane pump. Therefore, it is important to consider both the gases contained in the oil and the rotation movement of the vane chamber.

This paper reports on detailed measurements to confirm internal phenomena of the pump, and discusses the results of CFD analysis using a two phase homogeneous fluid model of gas-containing oil.

1 Introduction

In response to the increasing demand for improved fuel consumption of vehicles, needs to reduce the size of components, such as in-vehicle power steering systems and hydraulic vane pumps used in the CVT (Continuously Variable Transmission) system, are also increasing with the aim of reducing energy loss. Furthermore, higher rotating speed of the pump is also required in order to maintain pump characteristics. In light of this situation so far, we strive to enhance the characteristics in vane pump design and development by utilizing prototype evaluation [1] based on development experience and knowledge as well as CFD analysis. However, when a pump rotates at high speed, suction failures can easily occur due to steam caused by cavitation in the oil and the large amount of gases in oil, which is a unique requirement for the CVT system. In designing and developing of the vane pump, intricate modifications are required more than ever in, for example, oil flow design in suction channel in order to overcome such issues. It has reached the point in which such requirements cannot be met with conventional design technologies alone. Due to this, sophistication of CFD analysis technologies, such as prediction of the amount and behavior of gases in the hydraulic oil, is required in order to further improve pump characteristics. In recent CFD analysis, cavitation models [2) 3)] have been developed that consider gases precipitation and dissipation as well as gas-liquid two-phase flow models that consider gases and fluid have been developed. These technologies are being implemented in CFD analysis software (ANSYS®/Fluent and PumpLinx®, for example) in the market. In addition, implementations of rotational movement of vane chamber, and prediction of the amount and behavior of gases, which are required in design and development, have also been available for practical use by advancement of commercial analysis software. These technological advancements utilize many research achievements and findings, such as basic observation on cavitation mechanism [4)] and experimental verifications of CFD analysis accuracy [5) 6) 7) 8)]. Currently no investigation, however, has been done that characteristics prediction of vane pumps with the premise that a large amount of gases is contained within hydraulic oil, nor experimental investigation of such conditions.

In this review, we would like to explain technologies that KYB as a pump manufacturer continues to develop with the aim of overcoming above mentioned issues. By focusing on when pump rotates at high speed, especially, we would like to introduce the CFD analysis of the amount and behavior of gases in hydraulic oil as well as experimental evaluation results on prediction accuracy of CFD. Finally, we would also like to mention our discussion on the relationship between gas behaviors in pumps and pump characteristics.

2 Comprehending Experimental Phenomena

2.1 Vane pump

The pump for the test is a balanced-type vane pump and its structure is shown in Fig. 1. The rotary parts of the pump are 12 vanes, a rotor, and a shaft. The 12 vanes and a rotor are located between two valve plates with some notches.

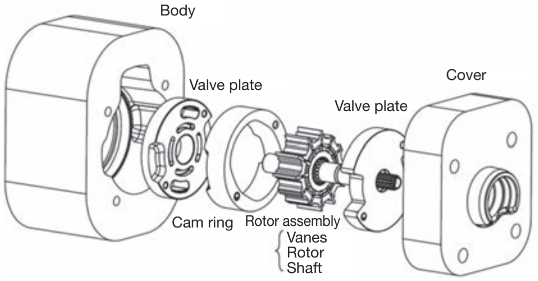

Fig. 1 Structure of the vane pump

2.2 Experiment circuit

As shown in Fig. 2, the hydraulic circuit used in the experiment is composed of the following three components.

(A) Circuit to measure the characteristics of the pump
(B) Circuit of gases mixing into oil inside the tank
(C) Circuit to measure the gas-injecting amount

Below is the explanation for these hydraulic circuits.

2.2.1 (A) Circuit to measure the characteristics of the trial pump

The characteristics between rotational speed and flow rate were measured with a volumetric flow meter installed on the pump delivery line, by using a servo motor to control the rotational speed of the pump. The oil temperature was that of oil inside the tank, and it was consistently controlled.

To measure the internal pressure in the vane chamber, pressure transducers was incorporated in the rotary parts, as shown in Photo 1. The lead wires from the pressure transducer are passed through a long narrow hole in the shaft, and then are connected onto the slip ring through the inside of the mechanical coupling (Fig. 3). Since the slip ring is a brush type, heat at the brush's rotational contact face is generated, causing a pressure measurement error due to change in electrical contact resistance. Therefore, we secured the measurement accuracy with preventing the heat generation during experiment by cooling down the temperature with air from an external blower.

2.2.2 (B) Circuit of gases mixing into oil in the tank

If gas is injected into the oil inside the tank, the gas in the oil do not instantly dissolve but remain as bubbles [4]. The bigger the bubble is, the more it tends to float due to

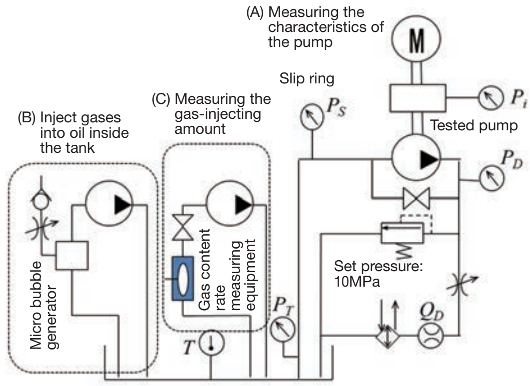

Fig. 2 Experimental hydraulic circuit

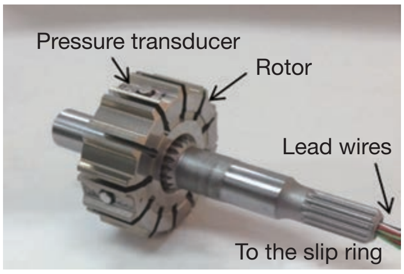

Photo 1 Pressure transducer for internal pressure measurement

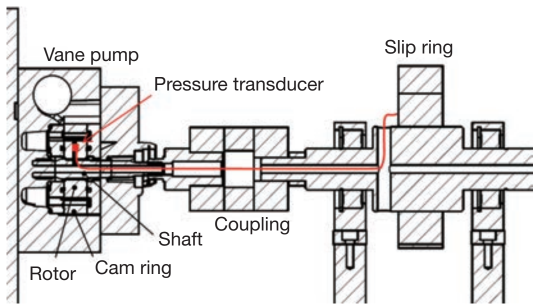

Fig. 3 Pressure transducer installation

buoyancy and dissipate toward atmosphere quickly. In the experiment, we therefore prepared a separate circulation circuit in order to retain bubbles within the oil in the tank and control a condition in which the bubbles are contained evenly. In this circuit, a micro bubble generator (bubble size: 10-30μm) was installed on the suction line of the circulation pump to inject micro bubbles in the oil. The amount of gas within oil (gas content rate) was adjusted with the amount of gas sent through the micro bubble generator. By breaking in the device prior to the experiment, we ensured that the gas content rate within the circuit was made consistent.

2.2.3 (C) Circuit to measure the mixed gas amount

The gas content rate is conventionally conducted by sampling oil from the tank with a syringe and measuring the gas volume with a measuring cylinder. However, using a syringe can cause gas precipitation and dissolution due to pressure changes, affecting the gas content rate.

Therefore, in this experiment, we measured the gas content rate in the tank on a real-time basis by connecting measuring equipment (Table 1), which can measure the gas content rate from oil impedance, to the hydraulic tank. This measuring method utilizes the fact that the sum of oil admittance Y_{OIL} and gas admittance Y_{GAS} in the sensor part is constantly conserved according to formula (1). Concerning the hydraulic oil actually used in the experiment, the relationship between temperature and Y_{GAS} as well as Y_{OIL} was conducted in advance, and then the gas content rate within the oil was calculated based on the conducted value.

$$Y_{OIL}+Y_{GAS}=\text{Const.} \tag{1}$$

Table 1 Specifications of measuring equipment for gas content rate

Measurement range	0 to 100%
Reproducibility	+/-1%
Measured medium	Liquid
Temperature measurement	+/-0.1°C
Temperature range	20 to 180°C
Maximum pressure range	Maximum of 1 MPa

2.3 Experiment result (Rotation number-flow characteristics)

Fig. 4 shows the experimental result of characteristics between rotational speed and flow rate at an oil temperature of 55°C and delivery pressure of 2.5 MPa. The horizontal axis R is non-dimensionalized at the rotational speed R_{ref} when the flow rate is 5% less than the theoretical flow rate Q_{ref} against the measured rotational speed ($Q_D = (1 -0.05) Q_{ref}$). Vertical axis Q is non-dimensionalized at the theoretical flow rate Q_{ref} when the non-dimensional rotational speed R is 1.0 against the measured flow. The black line in the figure shows the experimental result when gas was not injected. The average value of gas content rate value was γ_0 (Details to be mentioned later). The green line shows the experimental result when gas was injected. The average value of gas content rate was γ_1. The dotted line is plotted the values obtained by subtracting the amount of contained gas from the theoretical flow rate of each gas content rate. Both the experimental results, when R is 1.0 or less, are slightly lower than each theoretical flow rate. This difference is occurred due to leakage with inside the pump. When R exceeds 1.0, however, the flow rate rapidly decreases. It is assumed that this is caused by lack of suction. Furthermore, the flow reduction of green line, when gas is injected, becomes greater.

Fig. 5 shows the experimental waveform of the gas content rate during the experiment. The fact that the gas content rate when gas isn't injected is γ_0 rather than 0% indicates that oil already contains gas in the normal state. On the other hand, the gas content rate when gas is injected was γ_1, which is approximately five times as much as γ_0.

Photo 2 shows the oil surface conditions of the tank during the experiment. In Photo (b), we can observe white microscopic gas in the oil as a result of gas being injected.

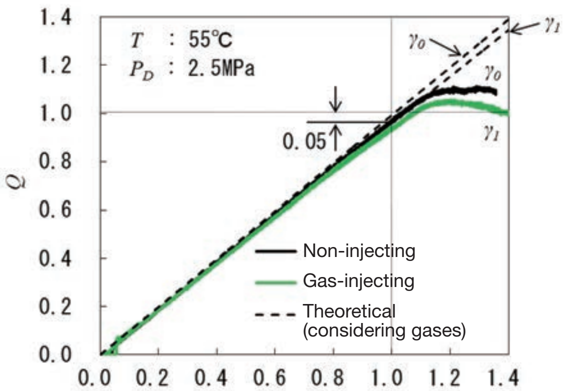

Fig. 4 Characteristics between rotational speed and flow rate

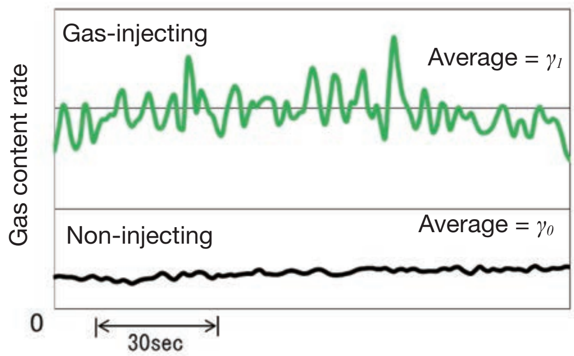

Fig. 5 Measurement results of gas content rate

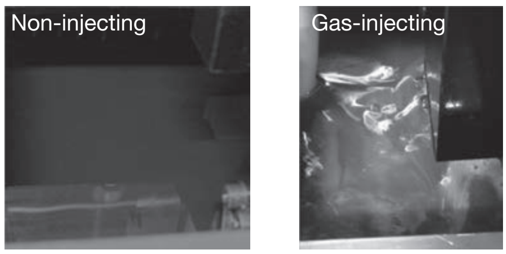

(a) Gas content rate γ_0 (b) Gas content rate γ_1

Photo 2 Oil surface condition in the tank

2.4 Experiment result (internal pressure in the vane chamber)

Next, we focused on one vane chamber in the pump with a fixed rotational speed without gas injected (gas content rate = γ_0) and measured the internal pressure of a chamber from the suction process to the delivery process. Fig. 6 shows the result. When R is 1.0 or less, the change of internal pressure tends to be similar even though some difference in the composition of the pulsation. The internal pressure at R=1.2, however, does not rise even when the process transitions to the compression process after the suction process, indicating that the status inside of the vane chamber has changed compared to when *R* is 1.0 or less. It is assumed that cavitation vapor occurred due to the suction pressure decrease caused by high speed rotation and the gases in the oil simultaneously expanded, preventing a pressure rise with the compressibility of these gases.

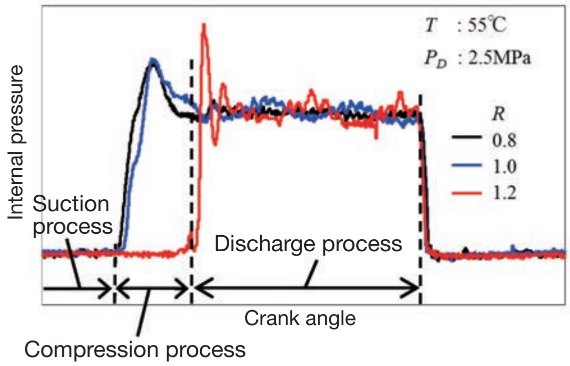

Fig. 6 Experimental results of internal pressure in vane chamber

3 CFD Analysis Technology

3.1 Conventional analysis technology (lumped constant model)

As a technology to predict the average of internal pressure in a vane chamber, we have developed a simulation tool [9) 10)] to predict the internal pressure of a vane pump by utilizing a lumped-parameter model. Prediction of the aforementioned experiment result based on this technology is as shown in Fig. 7. When we compare this to the experimental result in Fig. 6, we observe a great difference in the surge pressure when *R* is 1.2 (red line). Furthermore, pressure fluctuations in the delivery process are also not predicted. This is caused by the facts that it is difficult to determine gas behavior in the lumped-parameter model and that cavitation, which occurs in the vane chamber as mentioned in 2.4, cannot be predicted accurately. Therefore, predicting the internal pressure requires a CFD model that can high-accuracy simulate the gas behavior and status changes inside of the pump.

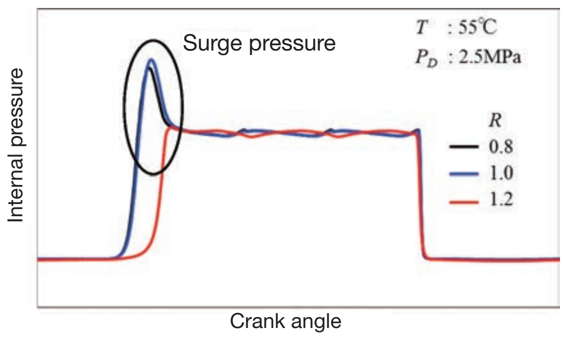

Fig. 7 Simulation results of internal pressure in vane chamber

Table 2 List of analysis setting

Fluid parameter			Unit
Oil	Temperature	55	°C
	Density	815	kg/m³
	Viscosity	0.0032	Pa/s
	Bulk modulus	1.52	GPa
	Vaporized pressure	400	Pa (Abs.)
Gas	Density	1.23	Kg/m³
	Viscosity	1.79×10-5	Pa/s
Boundary condition			
Entry pressure		0	MPa (Gage)
Discharge pressure		2.5	MPa (Gage)
Rotation number R		0.8 - 1.4	-
Mathematical model			
Two-phase flow		Homogeneous model	
Viscosity		Non-turbulent	
Cavitation		Singhal model	
Computational Grid			
Moving boundary		Sliding mesh method	
Vane chamber		Hexahedral grids	
Other		Tetrahedral grids	
Size of the smallest cell		1 x 10-5	m
Total number of cells		Approximately 3 million cells	
Calculation			
CPU (64bit PC)		E5-1650V3, 32GB RAM	
Time		2-4 days	

3.2 CFD analysis

For the CFD analysis, we utilized commercial software PumpLinx® (by Simerics). Table 2 shows a list of major analysis settings.

In this analysis, we handled two-phase flow as a homogeneous model by using the Singhal model to predict the cavitation. Furthermore, we also considered the rotational motion of the vane chamber in the unsteady analysis. Due to the fact that the grid shape changes along with rotation in this vane chamber model, we used hexahedral grids with the aim of reducing the calculation load and improving the analytical accuracy. Fig. 8 shows an example of computational grid using in the analysis. The number of the computational grids in this analysis was approximately three million cells, and the vane chamber covers approximately 30% of the overall cells. We also ensured accuracy by dividing finer the computational grids with a high rotational speed range.

3.3 CFD results (characteristics between rotational speed and flow rate)

The analysis model of CFD is the vane pump same as

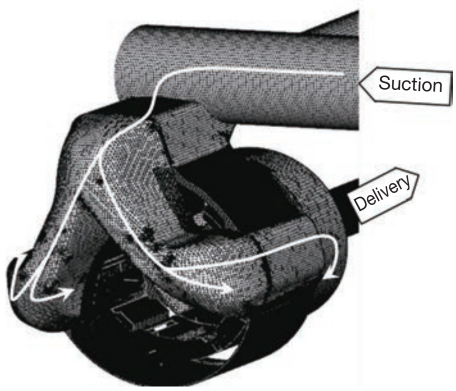

Fig. 8 Computational grids

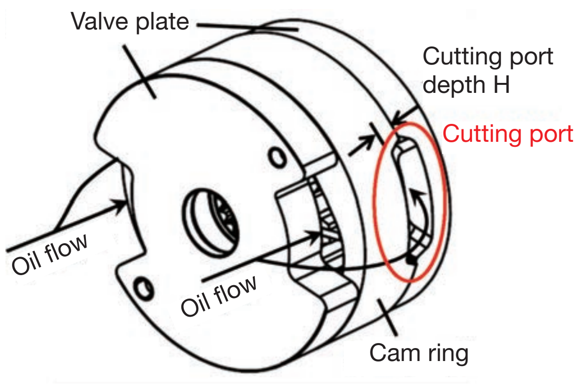

Fig. 9 Cutting port on cam ring

the experiment, indicated in Fig. 1. We used the cam ring cutting port (Fig. 9), which makes the oil channel to the vane chamber, as a parameter and compared the results. Cam ring without a cutting port is Type A, and two types of cam rings with a cutting port are Type B and Type C in Fig. 10. In addition, the depth of the cutting port is different between cam rings Type B and C. Type C's cutting port was twice as deep as Type B. We used these three cam rings and conducted a CFD analysis without gas injected in oil (gas content rate = γ_0) in order to obtain the per-rotation average of the delivery flow rate. With cam ring Type A, the CFD result without consideration for the cavitation model is plotted with outlined circles in Fig. 11. This is close to the dotted line, which expresses the theoretical flow without cavitation, and was not agreement with the experimental result (black line) in the high-speed rotation region. Therefore, we decided to conduct the analysis by considering the cavitation model next. As a result, we can see that the result drawn with black dots efficiently reproduces the experiment result, even with significant flow reduction when R is 1.0 or above.

In the same manner, the experiment/CFD result of cam rings Type B and C are individually shown in purple and orange. With these cam rings, the flow increased when R was 1 or above in the high-speed rotational region, compared to Type A. You can see that the CFD result was also predicted with high accuracy. In addition, the flow rate difference caused by cutting port depth was small both in the experimental result and in the CFD result.

Next, Fig. 12 shows the result in which gas was injected into oil (gas content rate = γ_1). The experimental result and CFD result were seen to be approximately the same in this case as well. With gas injected in oil, the effect of the cam ring became more obvious. A difference in the flow rate occurred (when R was 1.1 or above) due to be dependent on the cutting depth, which was not seen in Fig. 11. We can also see that the pump of Type C suctions more oil compared to the pump of Type B. As these results, you can see, CFD analysis with consideration of the cavitation model has enabled us to predict the experimental result with more accuracy with rotational speed-flow rate characteristics. Fig. 13 shows the flow prediction error

(a) Type A

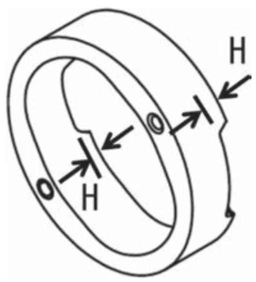

(b) Type B

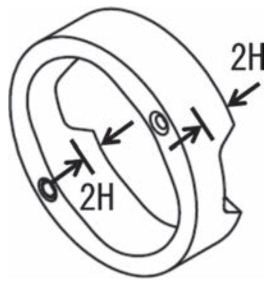

(c) Type C

Fig. 10 Configurations of cam ring

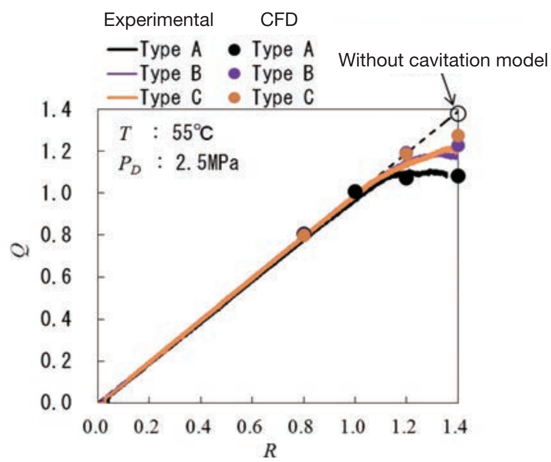

Fig. 11 Comparison of rotational speed-flow rate characteristics (Gas content rate γ_0)

with cam ring Type C when R is 1.4. Here, γ_2 is a gas content rate that is approximately 15 times more than γ_0. In each condition, the prediction was made with 5% or less error.

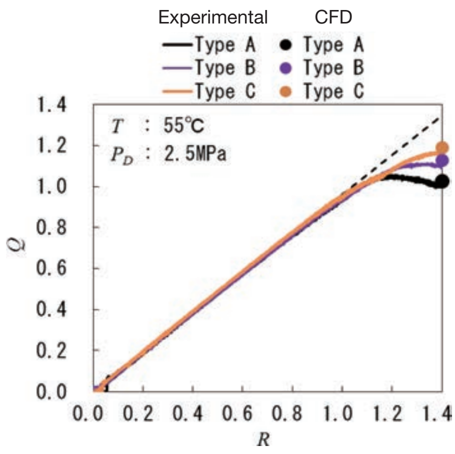

Fig. 12 Comparison of rotational speed-flow rate characteristics (Gas content rate γ_1)

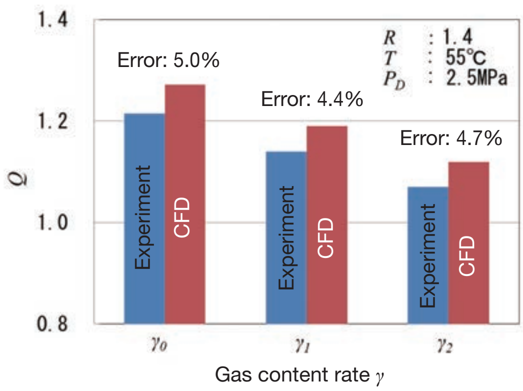

Fig. 13 Prediction error of flow rate by gas content rate

3.4 CFD results (internal pressure in the vane chamber)

The comparison of the experimental result and CFD result on the internal pressure in the vane chamber is shown in Fig. 14. The cam ring used for the experiment and analysis was Type C. Fig. 14 (a) is when the gas content rate is γ_0, and (b) is when the gas content rate is γ_2. When the experimental result and CFD result are compared, the surge pressure is greater in the CFD result. This is due to the fact that the leakage amount within the pump was not considered. In an actual pump, pressure decreases due to oil leakage from clearance, such as the tip of the vane and rotor side. The surge pressure is greater in the CFD analysis compared to the experiment. On the other hand, the lag behind in the pressure rising point and pressure fluctuations are relatively noticeable in the same manner as the experimental result. The prediction accuracy is improved compared to the lumped-parameter simulation.

Next, the gas content rate in the analysis is displayed in a contour diagram (Fig. 15) to analyze the gas status in the vane chamber. The vaporized pressure of the oil is the isosurface in this contour diagram. Fig. 15 shows the CFD result of the internal status of the vane chamber when R is 1.4. Fig. 15 (a) uses cam ring Type B, and (b) uses Type C. The area shown in the contour diagram is the area when gases are occurred, and warm color areas represent greater gas content rates. We can see in the figure that gases (cavitation) are generated when the rotation is faster due to the fact that the vane movement speed increases and the pressure for suction port decreases in both (a) and (b). With cam ring Type B, oil is not sufficiently filled with the vane chamber due to lack of suction. This causes the internal pressure of the vane chamber to decrease, remaining large clouds of gases toward the back of the vane. As a result, the amount of filled oil decreases, especially in areas away from the suction port (middle of the vane chamber), reducing the suction amount of the pump. On the other hand, by increasing the depth of the cutting port in cam ring Type C, it becomes easier for oil to be filled into the vane chamber compared to Type B. We have discovered that this reduces the gas clouds toward the back of the vane, increasing the oil suction amount.

As you can see, CFD analysis has enabled us to analyze even the state of gases inside of vane chambers. We can now consider theoretical designs to increase the rotational speed.

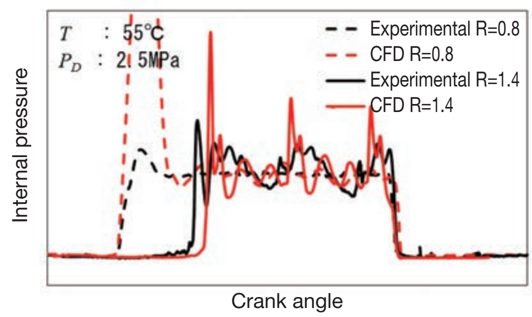

(a) Gas content rate: γ_0

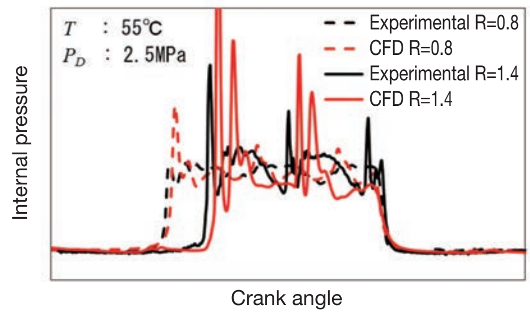

(b) Gas content rate: γ_2

Fig. 14 Comparison of internal pressure in vane chamber

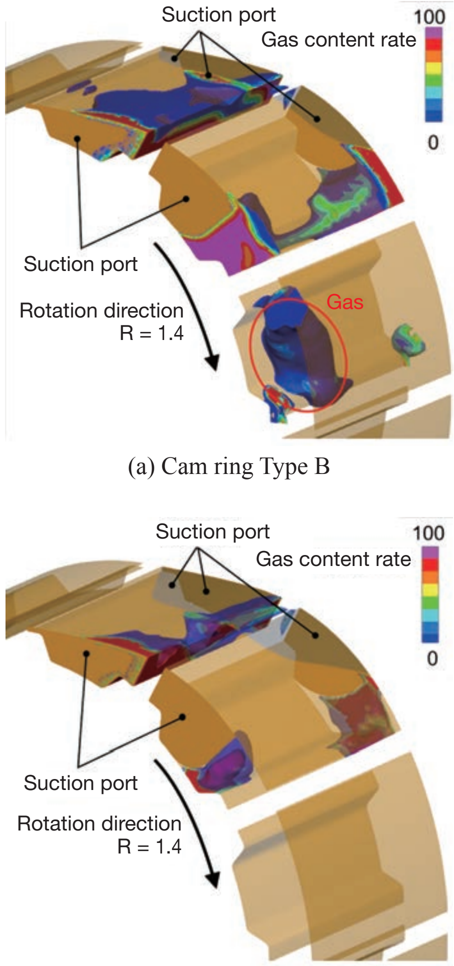

(a) Cam ring Type B

(b) Cam ring Type C

Fig. 15 Gas clouds in vane chamber

4 Concluding Remarks

In this review, we introduced our work with CFD analysis, including experimental verification, with the aim of improving vane pump performance by using the examples of rotational speed-flow rate characteristics and internal pressure of vane chamber.

Below are the results of these activities.

① We conducted a CFD analysis with consideration of gases in oil. This enabled us to conduct high-precision analysis on rotational speed-flow rate characteristics with 5% or less prediction error.

② We demonstrated in the experiment and analysis regarding vane chamber internal pressure that the pressure rising point is lagged behind as the pump rotational speed and gas content rate in oil increase.

③ We have discovered that the suction amount decreases due to the cavitation, which occurs in the suctioning process, and gases in the vane chamber during high-speed rotation.

In the future, we will promote the modeling of internal leakage in pump and parameters optimization of cavitation model in order to achieve higher accuracy on internal pressure prediction. In the future, we aim to contribute to the sophistication of vane pumps by applying the prediction technologies not only to driving torque but also quality characteristics, such as vibrations and noise.

References

1) Noguchi, E., Nagata, K., Evaluation Method for the Noise of Hydraulic Power-Steering System, FISITA World Automotive Congress, F2000H183, (2000).

2) Singhal, A. K., Athavale, M. M., Li, H., Jiang, Y., Mathematical Basis and Validation of the Full Cavitation Model, J. Fluids Eng., Vol.124, Issue 3, pp. 617-624, (2002).

3) Zwart1, P., Gerber, A., Belamri, T., A Two-Phase Flow Model for Predicting Cavitation Dynamics, ICMF 2004 International Conference on Multiphase Flow, No. 152, (2004).

4) Washio. S., Recent Developments in Cavitation Mechanisms, Elsevier Science & Technology, ISBN: 9781782421764, (2014).

5) Campo. D., et. Al., Numerical Analysis of External Gear Pumps Including Cavitation, Journal of Fluid Engineering, Vol. 134, Trans. of ASME, (2012).

6) Gao, H., Lin, W., Tsukiji, T., Investigation of Cavitation Near the Orifice of Hydraulic Valves, Proceedings of the Institution of Mechanical Engineers, Part G, Vol. 220, Journal of Aerospace Engineering, pp. 253-265, (2006).

7) Tsukiji, T., Nakayama, K., Saito. K., Yakabe. S., Study on the Cavitating Flow in an Oil Hydraulic Pump, Proceedings of 2011 International Conference on Fluid Power and Mechatronics, pp.253-258, (2011).

8) Suematsu, J., Tsukiji, T., Experimental and Numerical Flow Analysis in Hydraulic Vane Pump, Proceedings of KSFC2015 Autumn Conference on Drive & Control, pp. 3-7, (2015).

9) Nagata, K., Takahashi, K., Saito, K., A Simulation Technique for Pressure Fluctuation in a Vane Pump, 8th Bath International Fluid Power Workshop, pp. 169-183, (1995).

10) Yakabe, S., Nagata, K., Reduction of Pressure Fluctuation in a Vane Pump Using Genetic Algorithm, Fifth JFPS International Symposium, pp. 271-276, (2002).

Authors

SUZUKI Kazunari

Joined the company in 2008.
Mechanical component engineering Sect., Basic Technology R&D Center, Engineering Div.
Engaged in hydraulic equipment research and development and vibration/noise-related work.

NAKAMURA Yoshinari

Joined the company in 1997.
Specialist, Mechanical component engineering Sect., Basic Technology R&D Center, Engineering Div.
PhD (Engineering). Engaged in research and development that applies internal core technologies.

YAKABE Shinji

Joined the company in 1995.
Specialist, Mechanical component engineering Sect., Basic Technology R&D Center, Engineering Div.
Engaged in hydraulic equipment research and development and vibration/noise-related work.

WATANABE Hirohito

Joined the company in 1993.
Sagami Office, CAE Improvement Dept., Engineering Div.
Engaged in analysis work and CAE host control work.

NAKAMURA Kazuhisa

Joined the company in 2009.
Mechanical component engineering Sect., Basic Technology R&D Center, Engineering Div.
Engaged in hydraulic equipment research and development and vibration/noise-related work.